PHYSICAL REVIEW B VOLUME 15, NUMBER 5 1 MARCH 1977

Calculations of nuclear stopping, ranges, and straggling in the low-energy region*

W. D. Wilson and L. G. Haggmark
Theoretical Division, Sandia Laboratories, Livermore, California 94550

J. P. Biersack
Hahn-Meitner Institut, Berlin 39, Germany
(Received 21 June 1976)

Recent experimental results indicate that existing theories of low-energy nuclear stopping power based upon statistically derived potentials, such as the Thomas-Fermi potential, are in error by over 100%. This paper shows that these errors can be reduced to less than 10% by using more realistic interatomic potentials. We have calculated interatomic potentials from first principles in the free-electron approximation for 14 diatomic interactions representing light particles incident on heavy targets ($M_1 \ll M_2$), self-irradiation ($M_1 = M_2$), and heavy particles on light targets ($M_1 \gg M_2$). The potentials were approximated by a Molière-like form and the parameters tabulated for general covenience. The classical orbit equation was integrated numerically for bare potentials and the scattering cross section, stopping power, range, and straggling calculated. Simple three-parameter expressions for the stopping power are given which are directly integrable to obtain the range. The results are in reasonable agreement with experiment for a representative Kr-C potential and agree within 10% for an average potential derived from the free-electron calculations.

I. INTRODUCTION

Stopping powers and ranges of low-energy particles became a field of wide interest in the early 1960's, when Firsov[1] and Lindhard, Scharff, and Schiøtt[2] introduced their solutions, and when the first range measurements were performed. These first experiments obtained range information by implanting radioactive atoms, and then determining their depth distribution by stripping off layers of material by electrochemical[3] or physical methods.[4] Also, some of the early range data were obtained using a photoparticle recoil atom technique.[5] The depth resolution of these methods was sufficient to test the theory at reduced energies, ϵ, above $\epsilon \simeq 0.03$. Although satisfactory agreement was achieved in the higher-energy range $0.3 \leq \epsilon \leq 5$, the experimental range data tended to be somewhat higher than theoretical predictions in the lower-energy region, $0.03 \leq \epsilon \leq 0.3$, where deviations of more than 30% were observed. This trend was confirmed beyond doubt by recent measurements with improved techniques. Keinonen *et al.*[6] have already reported similar 30% discrepancies in stopping power and range values near $\epsilon = 0.3$, and Kalbitzer *et al.*[7,8] recently extended their stopping-power and range measurements down to $\epsilon = 0.0006$, resulting in ranges 100% above theoretical procedures.

Such deviations are serious enough to reconsider the underlying theoretical assumptions and procedures. Lindhard *et al.*[9] acknowledge that their treatment is inaccurate for $\epsilon < 10^{-2}$: "where deviations from Thomas-Fermi estimates may be considerable." Other simplifications incorporated in their treatment, such as combining energy and scattering angle into one variable as prescribed by the momentum approximation, do not account for more than about 20% deviation in the stopping power; this was shown earlier[9,10,22] by comparing the Lindhard *et al.* results with a rigorous computation based on a Thomas-Fermi potential. Another source of the observed discrepancy is the potential itself. This paper examines this source by presenting calculations of stopping powers, ranges, and stragglings for more realistic interatomic potentials.

In contrast to the Thomas-Fermi potential used in the existing theories, a realistic diatomic repulsive potential should drop to zero rather sharply for atomic separation greater than about 1 A, thus reducing atomic scattering at large impact parameters drastically. This would have the desired effect of reducing the nuclear stopping power and increasing particle ranges particularly at low energies. This can be accomplished by the introduction of an arbitrary cutoff in the potential-energy curve,[10] but then the choice of cutoff becomes the critical issue. Alternatively, realistic diatomic potentials determined from first principles are now available even for high-Z elements.[11,12] By using these more accurate potentials, we have developed a more fundamental and meaningful theoretical approach.

Our theoretical approach is presented in the remaining four sections of this paper. In Sec. II we discuss the interatomic potentials and present our results for 14 diatomic interactions. In Sec. III the classical scattering equation is solved and the stopping powers and average square fluctuations

in the energy loss are calculated. Analytical expressions for these quantities are presented in Sec. IV together with results for the range and range straggling. Section V contains a discussion of the results and the agreement with experiment.

II. INTERATOMIC POTENTIALS

A. Method of calculation

Because of their universal applicability, statistical models of interatomic interaction have been employed widely in all treatments of nuclear stopping power. Amongst the most notable of these interactions is the Sommerfeld approximation to the Thomas-Fermi potential,[13] the Molière approximation,[14] and the Bohr potential.[15] Each of these potentials is expressed as a Coulombic $(1/r)$ term multiplied by a "screening" function; interatomic distances are expressed in units of a screening length. In this way, the interaction can be universally applied if the screening function is known. The advantage of convenience, however, is somewhat lost in the lack of accuracy or at least in the lack of knowledge about the accuracy of the statistical model. Since other more accurate methods of interatomic potential determination exist, the application or need for better accuracy should provide the motivation for choosing between them.

The interactions between atoms comprising a solid can be obtained by assuming a parametrized functional form for the interaction and fitting the parameters to crystal data such as phonon disperion curves, elastic contants, compressibility, and lattice constant. These methods have been reviewed by Johnson.[16] Their obvious drawback is their lack of universal applicability and, more importantly for our purposes, the fact that they give accurate information about the potential only near the crystal-lattice spacing rather than in the repulsive region of interaction. It is impossible to extrapolate a potential obtained from such a parameter-fitting process to small interatomic separations without other information. Another disadvantage in this approach is that these potentials give information only for like-atom stopping powers (e.g., Nb in Nb). Other fitting procedures such as complete-neglect-of-differential-overlap exist and are applied where information about bonding is required.[17] For our purposes, they suffer from the same inability to give information over the entire range of interatomic separations as potentials obtained from crystal data.

At the other extreme of computational difficulty are methods such as Hartree-Fock and extensions thereof (such as multiconfigurational self-consistent-field methods). When correlation is included, these methods are clearly the most accurate known over the entire range of interatomic separations. They allow one to treat excited and ionized states also. Generally, they are applied where bonding effects are being studied. They are overly sophisticated (and consume enormous amounts of computer time) for studies on the repulsive region of the interatomic potential curve. The computational time, particularly for many electron systems, can be prohibitive although pseudopotential techniques are currently being developed to reduce the problem of approximating the core electrons.[18]

We must keep in mind that it is the low-energy repulsive region of the interatomic potential that is most important for nuclear stopping calculations. We employed the free-electron method referred to earlier[11] in this region because it has the advantage of being computationally simple and fast and gives better agreement with experiments compared even with methods at the Hartree-Fock level of accuracy. Briefly, atomic charge densities are calculated using the free-electron approximation and the interaction of the two atoms are obtained from classical electrostatics. Quantum-mechanical corrections for the increase in exchange and kinetic energy are made in the overlap region. Because the exchange energy is treated statistically in the Slater approximation, a form of correlation is taken into account as well. A similar method developed by Gordon and Kim[12] explicitly includes correlation. They find the dependence of the exchange and correlation energies on interatomic separation to be similar; that is, an overestimation of the exchange is somewhat equivalent to including correlation in such a model. For this reason, Wilson and Bisson[11] find their free-electron method of calculation to agree better with molecular-beam scattering experiments than Hartree-Fock calculations for all rare-gas pairs.

The method developed for rare gases was evaluated by comparing calculated helium interactions with other theoretical and experimental results. Results for He-Cu^+ free-electron interactions were found to agree reasonably with more sophisticated techniques.[19] Activation and binding for helium complexes in tungsten and lattice locations of helium in certain of these complexes are found to be consistent with experiment using these potentials. However, note that the systems studied involve rare gases which have closed-shell electronic configurations. The extension of this method to open-shell configurations must be approached with some caution, although for our purposes it is believed to provide reasonably realistic results.

Caution need also be exercised in choosing electronic configurations for the low-energy stopping

calculations. That is, questions of the possibility of electron stripping at the surface, electron "pickup" during the slowing-down process, and the charge state of the interacting species are difficult to resolve. Although, for example, a low-energy helium atom in aluminum may be considered neutral with a fair degree of confidence, it is far from clear whether this helium atom interacts with cores alone ($He\text{-}Al^{+++}$) or whether the valence electrons are equally important ($He\text{-}Al^{0}$). For this reason, several of our calculations were performed with varying charge states, to at least give an estimate of the importance of these effects. The electronic state of the projectile is assumed always to be the ground state although it is recognized that inelastic collisions even at low energies may modify this somewhat.

B. Results

We have chosen the free-electron method of determining interatomic potentials[11] for the reasons described above. In order to study a range of atomic numbers and masses, the He-Be, He-Al, He-Nb, He-Er, Al-Al, Nb-Nb, Kr-C, and Kr-Si potentials were calculated. Because the calculational method is incapable of handling bonding effects, only the energy region about ~1 eV is considered accurate. As mentioned above, the calculations were also performed for the ionized species Al^{+++}, Nb^{++}, and Er^{++}. For ease in reporting the results and also for utilitarian purposes, we have expressed the interatomic potential $V(r)$ as

$$V(r) = (Z_1 Z_2 e^2/r)\phi(r), \tag{1}$$

where r is the interatomic separation, e is the electronic charge, and Z_1, Z_2 are the atomic numbers of the elements involved. The function $\phi(r)$ is a screening function given by,

$$\phi(r) = \sum_{i=1}^{3} C_i e^{-b_i r/a}, \tag{2}$$

where a is a screening length,[1]

$$a = 0.8853 a_0/(Z_1^{1/2} + Z_2^{1/2})^{2/3} \tag{3}$$

(a_0 is the Bohr radius; Z_1 and Z_2 are the atomic numbers of the elements involved). The coefficients were restricted such that,

$$\sum_{i=1}^{3} C_i = 1$$

following Molière.[14] Table I gives the parameters C_i and b_i determined from a least-squares fit to the calculated free-electron potentials for each interaction along with those of the Molière function for comparison purposes. Also given in Table I is a set of C_i's and b's determined from least-squares fitting the combined set of *all* the *neutral* atom interactions. We consider this "averaged" set of parameters to represent a realistic screening function for the universal calculation of nuclear stopping powers.

In Fig. 1(a) we have plotted our calculated screening function versus dimensionless distance

TABLE I. Screening functions [Eq. (2)] for free-electron interatomic potentials. In determining the fits, only the actual calculated energies above 1 eV were included.

	C_1	C_2	C_3	b_1	b_2	b_3
$He\text{-}Be^{0}$	0.024 829	0.827 418	0.147 752	0.103 251	0.749 127	2.905 352
$He\text{-}Al^{0}$	0.050 859	0.695 714	0.253 427	0.229 291	0.620 437	2.426 450
$He\text{-}Nb^{0}$	0.289 907	0.429 335	0.280 758	0.322 526	0.770 095	2.432 938
$He\text{-}Er^{0}$	0.290 098	0.535 391	0.174 511	0.309 837	0.871 240	3.630 057
$Al^{0}\text{-}Al^{0}$	0.259 466	0.697 444	0.043 090	0.321 063	0.931 563	9.845 565
$Nb^{0}\text{-}Nb^{0}$	0.100 143	0.471 977	0.427 880	0.220 345	0.498 902	1.512 407
Kr-C	0.190 945	0.473 674	0.335 381	0.278 544	0.637 174	1.919 249
Kr-Si	0.096 029	0.444 825	0.459 146	0.234 088	0.502 060	1.399 874
$He\text{-}Be^{++}$	0.116 492	0.832 155	0.051 352	0.792 330	0.792 331	5.651 933
$He\text{-}Al^{+++}$	0.142 110	0.661 703	0.196 187	0.601 562	0.601 562	3.460 996
$He\text{-}Nb^{++}$	0.423 599	0.510 683	0.065 718	0.370 404	1.255 927	6.865 022
$He\text{-}Er^{++}$	0.402 713	0.547 287	0.049 999	0.346 327	1.269 632	10.831 888
$Al^{+++}\text{-}Al^{+++}$	−0.040 993	0.944 189	0.096 804	0.003 447	0.743 977	0.003 454
$Nb^{++}\text{-}Nb^{++}$	0.002 605	0.273 088	0.724 307	0.002 526	0.300 261	0.955 362
Average [a]	0.006 905	0.166 929	0.826 165	0.131 825	0.307 856	0.916 760
Molière [b]	0.35	0.55	0.10	0.3	1.2	6.0

[a] Least-squares average (~10% accuracy) to first eight interatomic potentials in this table [see Fig. 1(b)].

[b] Reference 14.

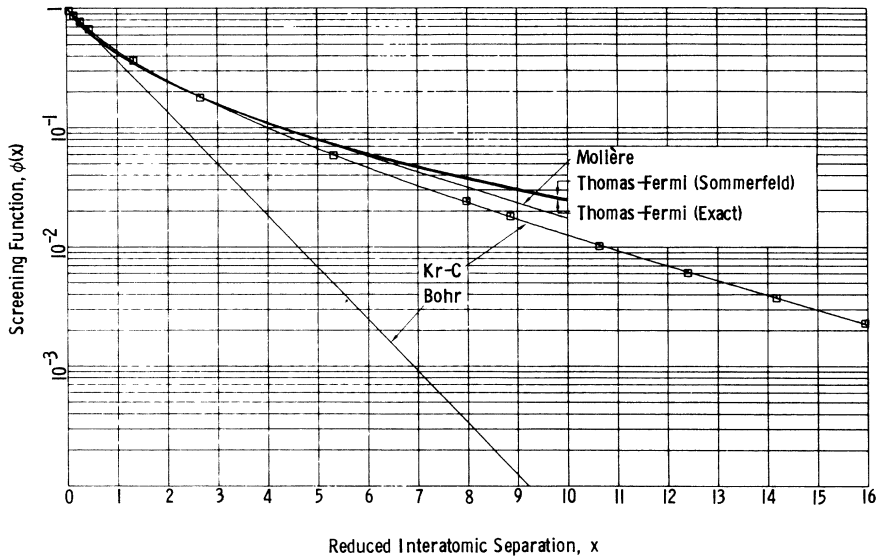

(a)

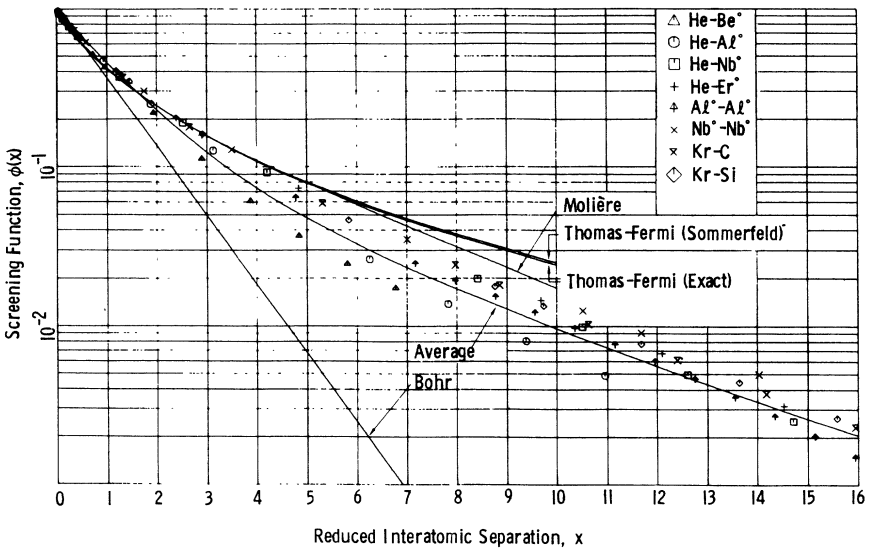

(b)

FIG. 1. (a) Comparison of the screening function for the free-electron Kr-C potential with those for the Thomas-Fermi, Molière, and Bohr potentials. Symbols for the Kr-C screening function represent the calculated points for potential energies >1 eV, and the line through these points represent the least-squares fit to a Molière-like screening function (see text and Table I). Thomas-Fermi (Sommerfeld) screening function is based on the values given by March (Ref. 25) and the Thomas-Fermi (exact) is based on the numerical evaluation of Kobayashi *et al.* (Ref. 26). (b) Comparisons of the screening functions for eight free-electron potentials with same general potentials as above. Each set of symbols represent the calculated points for a different neutral atom interaction for potential energies >1 eV. Solid line identified as average is the least-squares fit of all the points to a Molière-like screening function. Thomas-Fermi (Sommerfeld) screening function is based on the values given by March (Ref. 25) and the Thomas-Fermi (exact) is based on the numerical evaluation of Kobayashi *et al.* (Ref. 26).

$x(=r/a)$ for a representative case, Kr-C. The bare calculated points are shown along with the fit (see Table I); it is clear that the fit is quite reasonable. Also shown for comparison are the Thomas-Fermi, Molière, and Bohr potentials. The Bohr potential is seen to be too heavily screened, the Thomas-Fermi too weakly screened and, interestingly, the Molière potential lies closest to our calculated function. In the plot, and also in the parameters given in Table I, we chose to include only calculated values above 1 eV and to extrapolate the potential when required below this value. Including points between 1 and 0.1 eV had little effect on the results. We believe that this procedure is more meaningful than including calculated points in a region of the interatomic potential where binding and correlation effects dominate.

In Fig. 1(b) we show our calculated points (≥ 1 eV) for all the neutral atoms (first eight rows of Table I) and the least-squares fit to these values using the form given in Eq. (2). Note that the fitted curve gives a reasonable average of all the calculated results, but that deviations exist. For example, the curve lies somewhat above the calculated points for very small distances, $x \lesssim 1$, which will cause an ~10% deviation in the higher-energy stopping powers.

III. CALCULATIONS OF THE NUCLEAR STOPPING POWERS

The exact classical solution to the equation of motion of a particle moving in a central-force potential, $V(r)$, gives a scattering angle, θ, in the center-of-mass system given by

$$\theta = \pi - 2\int_{r_0}^{\infty} \frac{p\,dr}{r^2[1 - V(r)/E_c - p^2/r^2]^{1/2}}, \tag{4}$$

where p is the impact parameter, r_0 is the turning point (distance of closest approach) given by the root of the expression in the square root in Eq. (4), and E_c is the energy of the particle in the center-of-mass system. E_c is related to the initial kinetic energy, E, by

$$E_c = M_2 E/(M_1 + M_2),$$

where M_1 and M_2 are the incident- and target-atom masses, respectively. The differential scattering cross section, $\sigma(\theta)$ follows by differentiation

$$\sigma(\theta) = \frac{-p}{\sin\theta}\frac{dp}{d\theta}. \tag{5}$$

Note that θ and, therefore, $\sigma(\theta)$ are functions of the impact parameter and the particle energy.

For calculating the nuclear elastic scattering cross sections, which are necessary for determining the nuclear stopping power, we have employed the bare calculated values of the free-electron potentials (Sec. II) rather than the approximate analytical functions presented in Table I. Specifically, the numerical procedure consisted of calculating the diatomic interaction at ~30 points and then generating a finer mesh of values (500 points) by a cubic spline interpolation of the function $\ln[r\,V(r)]$. Because of the early work of Everhart *et al.*[20] we then performed a piece-wise fit of the potentials on the 500-point mesh to the screened-Coulomb form

$$V_i(r) = (A_i/r)e^{-r/B_i}, \tag{6}$$

where A_i and B_i are the fitted parameters between points i and $i+1$. We then solve Eq. (4) directly, using the method employed by Everhart *et al.*[20] As a check on our numerical procedures, we created accurate tabulations of the Thomas-Fermi (Sommerfeld), Molière, Bohr, and Born-Mayer potentials and calculated the scattering angles and cross sections for these potentials at several energies. A similar 500-point mesh was used, and our results compare very well (<1%) with Robinsin's[21] calculations of the turning points, scattering angles, and cross sections for these potentials

The nuclear stopping power dE/dR was obtained from

$$\frac{dE}{dR} = N\int_0^{T_m} T\,\sigma(T)\,dT, \tag{7}$$

where T is the energy transferred to the target atom, $T = \gamma E \sin^2\frac{1}{2}\theta$ and $\gamma = 4M_1M_2/(M_1+M_2)^2$, $\sigma(T)$ is the energy transfer cross section, T_m is the maximum energy transferred ($T_m = \gamma E$), and N is the atomic density of the target. The energy-transfer cross section is related to the scattering cross section by

$$\sigma(T) = (4\pi/\gamma E)\sigma(\theta). \tag{8}$$

The above nuclear stopping power can be expressed in terms of the reduced energy ϵ by using the following definitions:

$$S_n(\epsilon) = \frac{C}{\pi a^2 \gamma N}\frac{dE}{dR}, \tag{9}$$

for which

$$\epsilon = aM_2E/Z_1Z_2e^2(M_1+M_2) \tag{10}$$

and

$$C = \epsilon/E, \tag{11}$$

where a is the screening length [Eq. (3)] and Z_1e and Z_2e are the nuclear charges of the incident and target atoms, respectively. When converting the energy E into the reduced energy ϵ on both sides of Eq. (7), then the remaining parameters can be associated with the range R to define the reduced range ρ:

$$\rho = \pi a^2 \gamma N R. \tag{12}$$

By numerical integration of Eq. (7), the reduced nuclear stopping power, $S_n(\epsilon)$, has been determined for the Thomas-Fermi (Sommerfeld), Molière, Bohr, and 14 free-electron potentials presented in Sec. II. Our results for the Thomas-Fermi (Sommerfeld) potential are in excellent agreement ($\lesssim$0.1%) with the more exact calculations of Biersack.[22] Figure 2 shows $S_n(\epsilon)$ vs ϵ for the Thomas-Fermi (Sommerfeld), Molière, and Bohr potentials. Also included in this figure are the results for the free-electron Kr-C, Kr-Si, and average potentials, and the approximate results from the Lindhard *et al.*[9] theory. The results for the other potentials are displayed in Figs. 3–5. Note that the Thomas-Fermi potential predicts a high stopping power curve, consistent with its mild screening as seen in Fig. 1. Also note that the heavily screened (Fig. 1) Bohr potential gives a low estimate for the stopping power. The results for the Molière potential lie between these two extremes and closest to and somewhat above the realistic potential results for Kr-C and Kr-Si. These latter potentials give quite similar stopping powers. The Lindhard *et al.* results do not apply at very

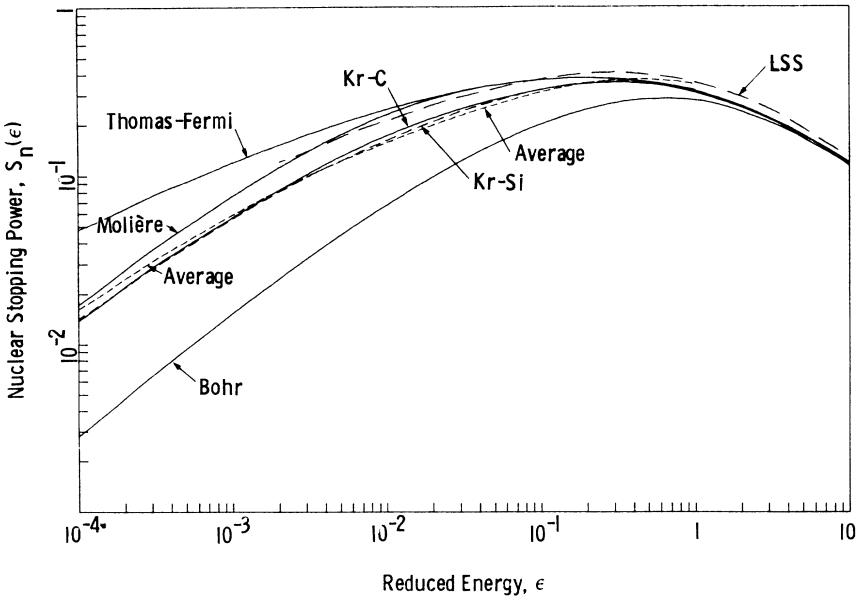

FIG. 2. Comparisons of the reduced nuclear stopping powers resulting from the Thomas-Fermi, Molière, and Bohr potentials with those resulting from the free-electron Kr-C, Kr-Si, and average potentials. Results from Lindhard, Scharff, and Schiøtt (LSS) theory are presented also for $\epsilon \gtrsim 0.002$.

low energies, but are given for comparison purposes for $\epsilon \geq 0.002$. The stopping power calculated from the average potential defined in Sec. II (Table I) is also shown to agree closely with the Kr-C and Kr-Si results. For all the diatomic cases considered, the Bohr potential gave a lower bound and the Molière gave an upper bound for the stopping power and, hence, these stopping powers are included in the figures.

The effect of the charge state on the low-energy stopping power is highly dependent upon atomic number as indicated in Figs. 3–5. For high-Z target elements (Nb and Er), the removal of two electrons has little effect on the stopping power. This is in contrast to the dramatic decrease in stopping power when low-Z elements (Be and Al) are considered to be in ionized states; that is, when cores alone are included in the interatomic potential calculation. We consider the neutral state to be more realistic at the low-energy extremes in which we are interested, in both cases, for the incident particle and for the target atoms.

We have also calculated the reduced average square fluctuation in the reduced energy loss, $W(\epsilon)$:

$$W(\epsilon) = \frac{C^2}{\pi a^2 \gamma^2} \int_0^{T_m} T^2 \sigma(T)\, dT \,. \tag{13}$$

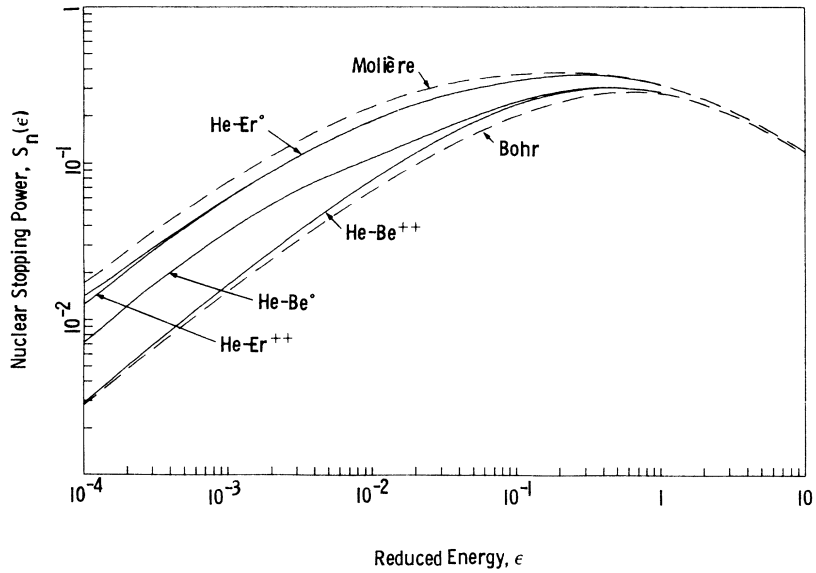

FIG. 3. Reduced nuclear stopping powers resulting from the free-electron He-Be^0, He-Be^{++}, He-Er^0, and He-Er^{++} potentials. Results for the Molière and Bohr potentials are repeated from Fig. 2 for reference purposes.

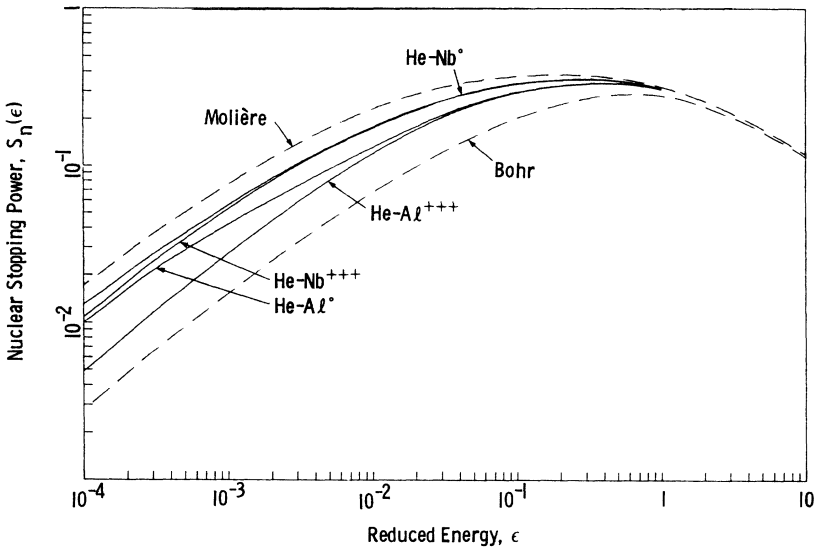

FIG. 4. Reduced nuclear stopping powers resulting from the free-electron He-Al^0, He-Al^{+++}, He-Nb^0, and He-Nb^{++} potentials. Results for the Molière and Bohr potentials are repeated from Fig. 2 for reference purposes.

All quantities having their earlier meaning. These calculations were performed for all the potentials discussed above and again, we obtain excellent agreement with the calculations of Biersack[22] for the Thomas-Fermi (Sommerfeld) potential. Representative results are given in Fig. 6 where it is seen that the Thomas-Fermi potential and the Bohr potential again give the extremes; the stopping power based on the Molière potential lies somewhat higher than, but closest to the average realistic potential and the Kr-C results.

IV. ANALYTIC EXPRESSIONS FOR $S_n(\epsilon)$, $W(\epsilon)$, $\rho(\epsilon)$, AND $f(t^{1/2})$

In order to make available the vast amount of information obtained through the methods described above, the results are presented in the form of analytic expressions rather than in elaborate tables or high precision graphs. This procedure also simplifies their further utilization in computer programs or other applications. Because of wide variation in results from the different interatomic potentials, the main emphasis in choosing analytic expressions is that they describe general trends properly rather than exactly reproducing the computational results. Such general features are

(a) Any stopping power formula for $\epsilon \gg 1$ must asymptotically merge into the form $S_n \approx (\ln\epsilon)/2\epsilon$ as required for Coulomb scattering.

(b) Any formula describing the increase of energy straggling per path length, must finally approach the value $W \approx \frac{1}{4}$ which results from Rutherford

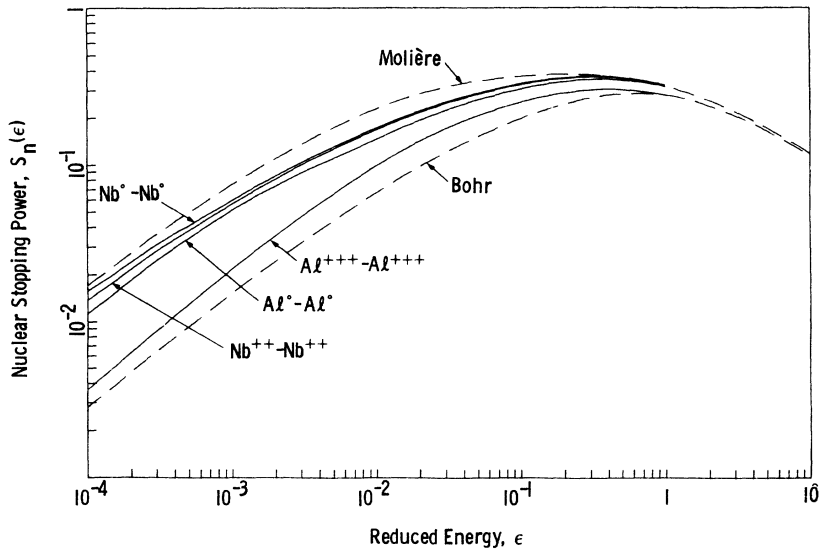

FIG. 5. Reduced nuclear stopping powers resulting from the free-electron Al^0-Al^0, Al^{+++}-Al^{+++}, Nb^0-Nb^0, Nb^{++}-Nb^{++} potentials. Results for the Molière and Bohr potentials are repeated from Fig. 2 for reference purposes.

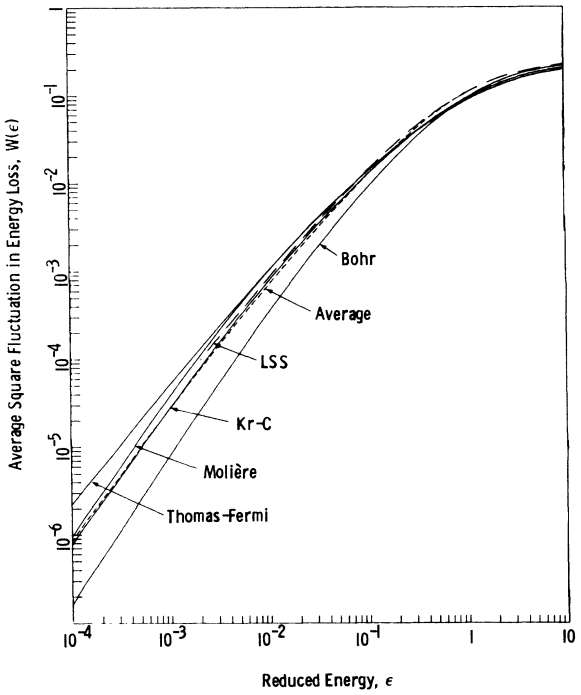

FIG. 6. Comparisons of reduced average square fluctuation in the reduced energy loss resulting from the free-electron Kr-C and average potentials with those resulting from Thomas-Fermi, Molière, and Bohr potentials. Results from the LSS theory are presented also for $\epsilon \geq 0.002$.

scattering at high energies.

(c) For very low energies, $\epsilon \ll 1$, the Thomas-Fermi potential acts as an r^{-4} potential, and consequently yields $S_n \sim \epsilon^{1/2}$ and $W \sim \epsilon^{3/2}$.

(d) For $\epsilon \ll 1$, all other potentials under consideration behave exponentially, or in terms of power-law fits, behave like r^{-n} with infinitely increasing values of n as ϵ approaches zero. This results in $S_n \sim \epsilon^{1-2/n}$ and $W \sim \epsilon^{2-2/n}$ with increasing n for $\epsilon \to 0$.

With these general features in mind, the following simple expressions are used:

$$S_n = [A \ln(B\epsilon)]/[B\epsilon - (B\epsilon)^{-C}], \tag{14}$$

$$S_n = [0.5 \ln(1+\epsilon)]/(\epsilon + A\epsilon^B), \tag{15}$$

$$W = 1/(4 + A\epsilon^{-B} + C\epsilon^{-D}). \tag{16}$$

Expressions (14) and (16) have been used by one of the authors earlier[23] for the description of Thomas-Fermi (TF) results. Formula (15) is added, as it leads immediately to simple estimates for both stopping power, $S_n \approx (1/2A)\epsilon^{1-B}$, and range, $\rho_n \approx 2A\epsilon^B/B$, for very low energies, $\epsilon \ll 1$. Further advantages of using analytic expressions rather than tables of numerical data are that they can be used more easily to determine range $\rho(\epsilon)$, relative range straggling, $(\langle \Delta\rho^2 \rangle / \rho^2)^{1/2}$, and the frequently employed $f(t^{1/2})$ function of the Lindhard theory. For example, from Eq. (14) one can obtain the range simply by integration of $1/S_n$:

$$\rho = \frac{E_1[(C-1)\ln(B\epsilon)] - E_1[-2\ln(B\epsilon)]}{AB} \quad \text{for} \quad B\epsilon < 1, \tag{17}$$

where

$$E_1(x) = \int_x^\infty \frac{e^{-y}}{y}\, dy;$$

for $B\epsilon \geq 1$ the electronic stopping process can no longer be neglected, cf. Eq. (19). Similarly, differentiation of the product $\epsilon S_n(\epsilon)$ yields

$$f = A\frac{X^{1+C} - 1 - (1+C)\ln X}{X^{2+C} - 2X + X^{-C}} \tag{18}$$

with $X \equiv Bt^{1/2} \equiv B\epsilon \sin\frac{1}{2}\theta$. This result determines the differential cross section in the Lindhard-Scharff-Schiøtt (LSS) approximation[2] since $d\sigma = 0.5\pi a^2 t^{-3/2} f(t^{1/2})\, dt$. However, it should be kept in mind that combining ϵ and $\sin\frac{1}{2}\theta$ into one single variable $t^{1/2}$ is an approximation which can result in considerable deviations from exact values, although it yields the correct stopping power, i.e., Eq. (14).

The constants to be used with Eqs. (14)–(18) have been calculated in a least-square sense from our numerical $S_n(\epsilon)$ and $W(\epsilon)$ results, and are listed in Table II for the Thomas-Fermi, Molière, Bohr, and Kr-C potentials. Also included is our average potential derived by a least-squares fit to all the neutral atom diatomic potentials combined (Table I). For the most part, the analytic expressions represent the actual results to within ~10% error. This deviation is not considered serious particularly when one considers the advantages of these expressions. It should be borne in mind that this ~10% deviation is the largest deviation found over five orders of magnitude in energy and that, furthermore, the expressions asymptotically approach the proper results beyond $\epsilon = 10$.

Turning our attention now to the range and relative range straggling, we define the reduced range

$$\rho(\epsilon) = \int_0^\epsilon \frac{d\epsilon'}{S_n(\epsilon') + S_e(\epsilon')}, \tag{19}$$

where $S_n(\epsilon)$ is the nuclear stopping power, given by Eq. (15) and $S_e(\epsilon)$ is the electronic stopping power. The inclusion of the electronic term allows a smooth transition to the region $\epsilon \gtrsim 0.1$, where S_e begins to become important. We used the approximation[2]

$$S_e(\epsilon) = k\sqrt{\epsilon}, \tag{20}$$

with the representative value, $k = 0.15$. In Fig. 7 we present the results of our calculations of the reduced range for various interatomic potentials by direct numerical integration of Eq. (19). In this figure we have also included $\rho_e(\epsilon)$ (reduced range based on the electronic stopping power only) for comparison purposes. Note that here we are calculating range along the particle path rather than projected range, and hence comparison with experiment should be restricted to heavy particles incident upon light targets. Calculation of the projected range requires a solution of the transport equation.

The relative range straggling was obtained from

$$\frac{1}{\gamma}\frac{\langle\Delta\rho^2\rangle}{\rho^2}=\frac{1}{\rho^2}\int_0^{\epsilon}\frac{W(\epsilon')\,d\epsilon'}{[S_n(\epsilon')+S_e(\epsilon')]^3} \tag{21}$$

and is tabulated for $0.0001 \le \epsilon \le 10.0$ in Table III for several potentials.

V. DISCUSSION AND RESULTS

The main results of this work are the stopping power and energy straggling curves, $S_n(\epsilon)$ and $W(\epsilon)$ for various diatomic potentials calculated from first principles and for some important "general" potentials for comparison. These results are presented in Figs. 2–6. The curves representing collisions between ions of higher

TABLE II. Fitted constants for Eqs. (14)–(16).

Potential	Constants				Largest deviation from actual calculation	
	A	B	C	D	%	At ϵ
			$S_n=\frac{A\ln(B\epsilon)}{B\epsilon-(B\epsilon)^{-C}}$			
Thomas-Fermi	0.494 71	1.3572	0.504 10		−2.7	1
					+2.9	0.0001
Molière	0.691 43	3.6013	0.713 52		−12.9	1
					+11.2	0.0001
Bohr	0.516 61	1.4821	0.832 73		−3.6	0.002
					+4.8	0.0001
Kr-C	0.598 18	2.1829	0.689 37		−7.3	1
					+9.2	0.0001
Average	0.562 58	1.1776	0.626 80		−6.6	0.002
					+8.0	0.0001
			$S_n=\frac{0.5\ln(1+\epsilon)}{\epsilon+A\epsilon^B}$			
Thomas-Fermi	0.103 96	0.507 93			−2.9	0.1
					+2.3	0.002
Molière	0.051 953	0.320 11			−1.7	0.001
					+3.9	0.5
Bohr	0.258 20	0.297 61			−4.2	0.0001
					+6.0	0.002
Kr-C	0.107 18	0.375 44			−2.7	0.05
					+4.1	0.0001
Average	0.141 20	0.420 59			−12.5	1
					+5.7	0.02
			$W=\frac{1}{4+A\epsilon^{-B}+C\epsilon^{-D}}$			
Thomas-Fermi	1.0329	1.4058	6.6276	0.826 46	−0.7	0.0005
					+0.8	0.0001
Molière	0.186 96	1.6828	6.9825	0.943 42	−0.5	0.5
					+0.5	1
Bohr	0.712 59	1.7311	7.2765	1.0555	−1.3	0.0005
					+1.5	0.0001
Kr-C	0.416 40	1.6192	6.4066	0.968 34	−2.1	0.2
					+1.9	1
Average	0.374 92	1.6119	4.9822	1.0965	−2.4	0.1
					+2.7	1

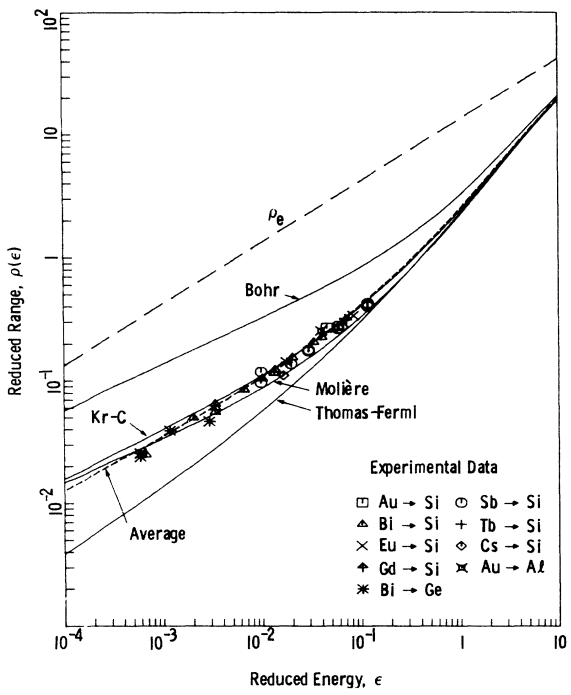

FIG. 7. Theoretical reduced range-energy curves compared to experimental data. Stopping power used is the sum of the individual nuclear and electronic stopping powers $S_e = 0.15\sqrt{\epsilon}$. Large dashed line labeled ρ_e is the reduced range based on electronic stopping only. Included is a set of recent data by Kalbitzer *et al.* (Refs. 7 and 8) representing low-enery range measurements of heavy ions incident on silicon, aluminum, and germanium. At higher energies these data merge smoothly into the multitude of other available data; e.g., Refs. 3 and 24, in complete agreement with theory.

charge state such as $Al^{+++} - Al^{+++}$ and $Nb^{++} - Nb^{++}$ are included in order to evaluate the influence of the outer electrons, but are not considered to represent realistic cases. All stopping power curves are seen to fall within the bounds given by the Molière (upper bound) and the Bohr potential (lower bound) but come somewhat closer to the Molière curve. The $W(\epsilon)$ curves depicted in Fig. 6 exhibit similar features as the $S_n(\epsilon)$ curves and need not be discussed separately.

From the stopping power and energy straggling results, we next calculate the range $\rho(\epsilon)$, and the relative range straggling $\gamma^{-1}\langle\Delta\rho^2\rangle/\rho^2$ for three general potentials (Molière, Bohr, and Thomas-Fermi), for one representative individual potential, and for the "average" realistic potential. The range and range straggling calculation which include electronic energy loss are depicted in Fig. 7 and Table III, respectively. For comparison, the experimental data of Kalbitzer *et al.*[7,8] is also presented in Fig. 7. These data are more indicative than exhaustive; for more detailed experimental information the reader is referred to the comprehensive monograph of Mayer *et al.*[24] The experimental range data depicted in Fig. 7 are projected ranges and should, therefore, be located slightly *below* the theoretical curve for range-along-path. Therefore, we consider that the agreement is excellent between the experimental data and our results for both the Kr-C and average potential.

We have demonstrated that interatomic potentials calculated from first principles in the free-electron approximation are sufficiently accurate to

TABLE III. Relative range straggling (multiplied by appropriate constants to make them dimensionless) calculated for several interatomic potentials, taking into account electronic losses by $S_e = 0.15\sqrt{\epsilon}$. $\langle\Delta\rho^2\rangle/\gamma\rho^2$ or equally $[(M_1+M_2)^2/4M_1M_2]\,(\langle\Delta R^2\rangle/R^2)$.

				Free-electron	
ϵ	Thomas-Fermi	Molière	Bohr	Kr-C	Average
0.0001	0.129	0.0855	0.0649	0.0960	0.101
0.0002	0.125	0.0864	0.0683	0.0963	0.102
0.0005	0.121	0.0877	0.0724	0.0968	0.103
0.001	0.120	0.0889	0.0751	0.0972	0.104
0.002	0.120	0.0904	0.0774	0.0977	0.104
0.005	0.123	0.0929	0.0796	0.0986	0.103
0.01	0.126	0.0955	0.0805	0.0996	0.103
0.02	0.130	0.0988	0.0808	0.101	0.104
0.05	0.133	0.104	0.0806	0.104	0.106
0.1	0.133	0.107	0.0805	0.106	0.110
0.2	0.129	0.109	0.0810	0.108	0.115
0.5	0.116	0.106	0.0826	0.106	0.119
1.0	0.101	0.0970	0.0815	0.0983	0.113
2.0	0.0804	0.0807	0.0736	0.0825	0.0956
5.0	0.0491	0.0509	0.0501	0.0522	0.0593
10.0	0.0288	0.0300	0.0305	0.0308	0.0342

predict the ranges of low-energy atoms in solids. We have, furthermore, demonstrated that these ranges are quite sensitive to the chosen potential and that the Molière approximation lies closest to our theoretical curves. The agreement with experiment is excellent although most of the data are for incident and target species differing somewhat from those chosen as representative cases here. We suggest that the appropriate calculated curves be used in comparing to experiment rather than our "average" potential because of their clearer meaning. The average potential, however, seems to give more realistic range and functional energy dependence than any other form (even Molière) where a universal potential is sought.

ACKNOWLEDGMENTS

It is a great pleasure to thank Dr. S. Kalbitzer, of the Max-Planck Institut für Kernphysik, Heidelberg, for the communication of experimental data prior to publication. We also wish to express our appreciation to C. L. Bisson, of Sandia Laboratories, for his assistance in the calculations of the free-electron potentials.

---

*Work supported by the U.S. Energy Research and Development Administration.

[1]O. B. Firsov, Zh. Eksp. Teor. Fiz. 32, 1464 (1957); 33, 696 (1957); 34, 447 (1958) [Sov. Phys.-JETP 5, 1192 (1957); 7, 308 (1958); 9, 1076 (1959)].

[2]J. Lindhard, M. Scharff, and H. E. Schiøtt, Mat. Phys. Medd. Dan. Vid. Selsk. 33, No. 14 (1963).

[3]J. A. Davies, G. A. Sims, Can. J. Chem. 39, 601 (1961); P. Jespersgaard and J. A. Davies, Can. J. Phys. 45, 2983 (1967), and references therein.

[4]H. Lutz and R. Sizmann, Phys. Lett. 5, 113 (1963); J. L. Whitton, Can. J. Phys. 46, 581 (1968).

[5]V. A. J. van Lint, M. E. Wyatt, R. A. Schmitt, C. S. Suffredini, and D. K. Nichols, Phys. Rev. 147, 242 (1966). See also V. A. J. van Lint, R. A. Schmitt, and C. S. Suffredini, Phys. Rev. 121, 1457 (1961); R. A. Schmitt and R. A. Sharp, Phys. Rev. Lett. 1, 445 (1958).

[6]J. Keinonen (private communication); also see M. Bister, A. Antilla, and J. Keinonen, Phys. Lett. A 53, 471 (1975).

[7]A. Feuerstein, S. Kalbitzer, and H. Oetzmann, Phys. Lett. A 51, 165 (1975); H. Oetzmann, A. Feuerstein, H. Grahmann, and S. Kalbitzer, *ibid.* 55, 170 (1975).

[8]S. Kalbitzer (private communication); also see H. Oetzmann, A. Feuerstein, H. Grahmann, and S. Kalbitzer, in *Proceedings of the International Conference on Ion Beam Surface Layer Analysis*, Karlsruhe, 1975 (Plenum, London, 1976), p. 245.

[9]J. Lindhard, V. Nielsen, and M. Scharff, Mat. Phys. Medd. Dan. Vid. Selsk, 36, No. 10 (1968).

[10]B. M. Latta and P. J. Scanlon, Phys. Rev. A 10, 1638 (1974).

[11]W. D. Wilson and C. L. Bisson, Phys. Rev. B 3, 3984 (1971).

[12]R. G. Gordon and Y. S. Kim, J. Chem. Phys. 56, 3122 (1972).

[13]A. Sommerfeld, Z. Physik 78, 283 (1932).

[14]G. Molière, Z. Naturforschung. A 2, 133 (1947).

[15]N. Bohr, Kgl. Danske Videnskab. Selskab. Mat.-Fys. Medd. 18, 8 (1948).

[16]R. A. Johnson, J. Phys. F 3, 295 (1973).

[17]J. N. Murrell and A. J. Harget, *Semi-Empirical Self-Consistent-Field Molecular Orbital Theory of Molecules* (Wiley-Interscience, London, 1971).

[18]See, for example, C. F. Melius and W. A. Goddard III, Phys. Rev. A 10, 1528 (1974).

[19]W. D. Wilson, Proceedings of the International Conference on "Fundamental Aspects of Radiation Damage in Metals," Gatlinburg, Tennessee, Oct. 1975 (unpublished).

[20]E. Everhart, G. Stone, and F. J. Carbone, Phys. Rev. 99, 1287 (1955).

[21]M. T. Robinson, publication of the Oak Ridge National Laboratory, Oak Ridge, Tennessee, Report ORNL-4556 (1970) (unpublished).

[22]J. P. Biersack, publication of the Hahn-Meitner Institut, Berlin, Report HMI-B37 (1964) (unpublished).

[23]J. P. Biersack, Z. Phys. 211, 495 (1968).

[24]J. W. Mayer, L. Erickson, and J. A. Davies, *Ion Implantation in Semiconductors* (Academic, New York, 1970).

[25]N. H. March, Proc. Cambridge Philos. Soc. 46, 356 (1950).

[26]S. Kobayashi, T. Matsukuma, S. Nagai, and K. Umeda, J. Phys. Soc. Jpn. 10, 759 (1955).